

Theoretical description of mixed-field orientation of asymmetric top molecules: a time-dependent study

Juan J. Omiste¹ and Rosario González-Férez²

¹*Department of Physics and Astronomy, Aarhus University, 8000 Aarhus C, Denmark*

²*Instituto Carlos I de Física Teórica y Computacional and Departamento de Física Atómica, Molecular y Nuclear, Universidad de Granada, 18001 Granada, Spain*

(Dated: Friday 27th July, 2018)

We present a theoretical study of the mixed-field-orientation of asymmetric top molecules in tilted static electric field and non-resonant linearly polarized laser pulse by solving the time-dependent Schrödinger equation. Within this framework, we compute the mixed-field orientation of a state-selected molecular beam of benzonitrile (C_7H_5N) and compare with the experimental observations [1], and with our previous time-independent descriptions [2]. For an excited rotational state, we investigate the field-dressed dynamics for several field configurations as those used in the mixed-field experiments. The non-adiabatic phenomena and their consequences on the rotational dynamics are analyzed in detail.

I. INTRODUCTION

During the last years, experimental efforts have been undertaken to develop and improve experimental techniques to enhance the orientation of polar molecules [3–8]. When a molecule is oriented the molecular fixed axes are confined along the laboratory fixed axes and its permanent dipole moment possesses a well defined direction. The experimental efforts are motivated by the broad range of promising perspectives and possible applications of oriented molecules, such as high-order harmonic generation [9–11], chemical reaction dynamics [12–15], ultracold molecule-molecule collision dynamics [16–19], and diffractive imaging of polyatomic molecules [20, 21].

The theoretical prediction to strongly orient molecules by coupling the quasidegenerate levels of a non-resonant-laser generated pendular state [22, 23], quickly became a promising experimental technique [24–26]. However, only using state-selected ensembles of linear and asymmetric top molecules unprecedented degrees of orientation could be reached [3, 4, 27, 28]. These experimental efforts have been accompanied of theoretical studies to provide a better physical insight into the field-dressed dynamics. For a state-selected beam of asymmetric top molecules, the first analysis showed that the experimental mixed-field orientation could not be reproduced in an adiabatic description [2]. Based on the lack of azimuthal symmetry due to the weak static electric field, a diabatic model was proposed to classify the avoided crossing as diabatic and adiabatic depending on the field-free magnetic quantum numbers of the involved states [2]. An explicit time-dependent analysis of the mixed-field-orientation experiments of OCS concluded that this process is, in general, non-adiabatic and requires a time-dependent quantum-mechanical description [29]. The lack of adiabaticity is due to the formation of the quasidegenerate pendular doublets as the laser intensity is increased, the resulting narrow avoided crossings, and the corresponding couplings between the states in a $|J, M\rangle$ manifold for tilted fields [29, 30]. These non-adiabatic phenomena provoke a

transfer of population between energetically neighboring adiabatic pendular states, which might significantly reduce the degree of orientation [29, 30], this effect can be mitigated using stronger dc electric fields [31]. This population transfer between the oriented and anti-oriented states forming a pendular doublet could be efficiently controlled to achieve a strong field-free orientation during the post-pulse dynamics [32].

For an asymmetric top molecule, we had performed a first time-dependent study on parallel fields showing the complexity of the field-dressed dynamics [33]. Here, we extend this work and analyze the rotational dynamics of benzonitrile (BN) in tilted-field configurations similar to those used in current mixed-field experiments. Within this time-dependent framework, we revisit the experiment on mixed-field orientation of a state-selected molecular beam of benzonitrile [1, 34], extending upon our earlier theoretical description [2]. The sources of discrepancies between the experimental results and the time-dependent description are analyzed. For a prototypical excited rotational state, we explore the field-dressed rotational dynamics and investigate the complicated non-adiabatic phenomena, showing that it is experimentally more challenging to reach the adiabatic limit.

The paper is organized as follows: In Sec. II we present the Hamiltonian of a polar asymmetric top molecule in tilted electric and non-resonant laser fields, and the numerical method used to solve the time-independent Schrödinger equation. The time-dependent description of the mixed-field orientation experiment of a benzonitrile molecular beam is presented in Sec. III, where we also provide a comparison with our previous time-independent analysis. Section IV is devoted to investigate the mixed-field dynamics of an excited rotational state, and we explore the sources of non-adiabatic effects in Sec. V. The conclusions are given in Sec. VI.

II. THE HAMILTONIAN OF AN ASYMMETRIC TOP MOLECULE IN TILTED FIELDS

We consider a polar asymmetric top molecule in combined electric and non-resonant laser fields. Our study is restricted to asymmetric top molecules that can be described within the rigid rotor approximation, and that have the polarizability tensor diagonal in the principal axes of inertia frame and the permanent electric dipole moment μ parallel to the z -axis of this molecule fixed frame (MFF) (x, y, z) . The MFF z -axis is taken along the molecular axis with the smallest moment of inertia. The non-resonant laser field is linearly polarized along the Z -axis of the laboratory fixed frame (LFF) (X, Y, Z) and the electric field is tilted by an angle β with respect to the LFF Z -axis and contained in the XZ -plane. The rotational dynamics of the molecule is described using the Euler angles (θ, ϕ, χ) that relate the LFF and MFF [35]. In the framework of the rigid rotor approximation, the Hamiltonian reads as

$$H(t) = H_R + H_s(t) + H_L(t), \quad (1)$$

where H_R is the field-free rotational Hamiltonian

$$H_R = B_x J_x^2 + B_y J_y^2 + B_z J_z^2 \quad (2)$$

with J_k being the projection of the total angular momentum operator \mathbf{J} along the MFF k -axis with $k = x, y$, and z , and B_k the rotational constant along the MFF k -axis. For BN, the rotational constants are $B_x = 1214$ MHz, $B_y = 1547$ MHz and $B_z = 5655$ MHz [36].

The electric field $E_s(t)$ interacts with the electric dipole moment μ of the molecule as

$$H_s(t) = -\mu E_s(t) \cos \theta_s, \quad (3)$$

where θ_s is the angle between the electric field and the MFF z -axis, $\cos \theta_s = \cos \theta \cos \beta + \sin \beta \sin \theta \cos \phi$. For BN, the permanent electric dipole moment is $\mu = 4.515$ D [36]. $E_s(t)$ initially depends linearly on time, and once the maximum strength E_s is reached, it is kept constant. The turning on speed ensures that the process is adiabatic, and we have neglected the coupling of this field with the molecular polarizability or higher order terms.

For a non-resonant linearly polarized laser field, the interaction reads [37, 38]

$$H_L(t) = -\frac{I(t)}{2\epsilon_0 c} (\alpha^{zx} \cos^2 \theta + \alpha^{yx} \sin^2 \theta \sin^2 \chi), \quad (4)$$

where $\alpha^{km} = \alpha_{kk} - \alpha_{mm}$ are the polarizability anisotropies, and α_{kk} the polarizability along the molecular k -axis $k, m = x, y$ and z . For BN, the polarizabilities are $\alpha_{xx} = 7.49$ Å³, $\alpha_{yy} = 13.01$ Å³ and $\alpha_{zz} = 18.64$ Å³ [36]. ϵ_0 is the dielectric constant and c the speed of light. In this work, we consider Gaussian pulses with intensity $I(t) = I_0 \exp\left(-\frac{4 \ln 2 t^2}{\tau^2}\right)$, I_0 is

Parity			Functions
C_z^2	σ_{XZ}	K	
e	e	$e, K, M = 0$	$ J00\rangle$
e	e	e	$\frac{1}{\sqrt{2}} (JKM\rangle + (-1)^{K+M} J-K-M\rangle)$
e	o	e	$\frac{1}{\sqrt{2}} (JKM\rangle + (-1)^{K+M+1} J-K-M\rangle)$
o	e	o	$\frac{1}{\sqrt{2}} (JKM\rangle + (-1)^{K+M} J-K-M\rangle)$
o	o	o	$\frac{1}{\sqrt{2}} (JKM\rangle + (-1)^{K+M+1} J-K-M\rangle)$

Table I. For tilted fields with $\beta \neq 90^\circ$, functions used in the basis set expansion of the time-dependent wave function.

the peak intensity and τ is the full width half maximum (FWHM).

For tilted fields with $\beta \neq 0^\circ, 90^\circ, 180^\circ$, the symmetries of the rigid rotor Hamiltonian (1) are the identity, E , the two fold rotation around the MFF z -axis, C_z^2 , and the reflections σ_{XZ} on the plane spanned by the two fields, i. e., the XZ -plane. These symmetries imply the conservation of the parity of the projection of \mathbf{J} on the MFF z -axis, i. e., the parity of K , and the parity under the reflections on the LFF XZ -plane σ_{XZ} . Consequently, the eigenstates can be classified in four different irreducible representations [38], whose basis elements are presented in Table I in terms of the field-free symmetric top eigenstates $|JKM\rangle$ [38].

The time-dependent Schrödinger equation associated with the Hamiltonian (1) is solved combining the short iterative Lanczos method [39] for the time variable and a basis set expansion in the field-free top eigenstates written in terms of the Wang states, $|JKM\rangle$, for the angular coordinates. For each irreducible representation, the symmetric top wave functions forming the basis are properly symmetrized as indicated in Table I [38]. The time-dependent wave function is labeled using the adiabatic following and the field-free notation $|J_{K_a, K_c} M\rangle_t$ where K_a and K_c are the values of K for the limiting prolate and oblate symmetric top rotor, respectively [40].

To analyze the rotational dynamics, the time-dependent wave function is projected on the adiabatic pendular states at time t

$$|J_{K_a, K_c} M\rangle_t = \sum C_{|\mathcal{J}_{K_a, K_c} \mathcal{M}\rangle}(t) |\mathcal{J}_{K_a, K_c} \mathcal{M}\rangle_p \quad (5)$$

with $C_{|\mathcal{J}_{K_a, K_c} \mathcal{M}\rangle}(t) = {}_p \langle \mathcal{J}_{K_a, K_c} \mathcal{M} | J_{K_a, K_c} M \rangle_t$ and the wave function of the adiabatic pendular state of the instantaneous Hamiltonian (1) $|\mathcal{J}_{K_a, K_c} \mathcal{M}\rangle_p$ that connects adiabatically to the field-free state $|J_{K_a, K_c} M\rangle$. The sum in Eq. (5) runs over all pendular states within the same irreducible representation.

The rotational dynamics can be characterized by the adiabaticity ratio or parameter [41]

$$\eta = \frac{\hbar \left| \left\langle k \left| \frac{\partial H_L(t)}{\partial t} \right| m \right\rangle_p \right|}{|E_m - E_k|^2} \quad (6)$$

where $|k\rangle_p$ and $|m\rangle_p$ are the eigenfunctions of the adiabatic pendular eigenstates of Hamiltonian (1) at time t and E_k and E_m are the eigenenergies. The rotational dynamics can be considered as adiabatic at a certain time if $\eta \ll 1$ [41].

A. Experimental measures

In mixed-field orientation experiments, the degree of orientation can be measured by a multiple-ionization and a subsequent Coulomb explosion of the molecule, and the velocity mapping of the ionic fragments onto a 2D screen perpendicular to the dc field of the velocity mapping electrodes. The molecular orientation is reflected in the 2D-images, which show an up/down asymmetry measured by the ratio $N_{\text{up}}/N_{\text{tot}}$, where N_{tot} and N_{up} stand for the amount of ions collected on the full screen and on its upper part, respectively, [3, 4, 27]. Theoretically, the recorded image corresponds to the 2D projection of the 3D probability density on the screen perpendicular to the electric field [2, 29]. The theoretical orientation ratio $N_{\text{up}}/N_{\text{tot}}$ reads

$$N_{\text{up}}/N_{\text{tot}} = \frac{\int_0^\infty \int_{-\infty}^\infty \rho(y_s, z_s) dy_s dz_s}{\int_{-\infty}^\infty \int_{-\infty}^\infty \rho(y_s, z_s) dy_s dz_s}. \quad (7)$$

where $\rho(y_s, z_s)$ is the 2D probability density, y_s and z_s are the horizontal and vertical screen coordinates, respectively. Here, we derive this 2D probability density including the selectivity factor of a circularly polarized probe laser and the experimental velocity distribution of the ionic fragments under the recoil approximation [2]. Note that for non-oriented states, $\langle \cos\theta \rangle = 0$ and $N_{\text{up}}/N_{\text{tot}} = 0.5$, whereas $N_{\text{up}}/N_{\text{tot}} > 0.5$ and $N_{\text{up}}/N_{\text{tot}} < 0.5$ for oriented and antioriented states, respectively.

III. MIXED-FIELD ORIENTATION FOR EXPERIMENTAL CONDITIONS

In this section we present a theoretical time-dependent description of the mixed-field orientation corresponding to previous mixed-field-orientation experiments of benzonitrile [27], and a comparison with our previous time-independent analysis [2]. State-selected benzonitrile molecules in a molecular beam were oriented using the weak dc electric field from the velocity-mapping spectrometer and a non-resonant laser pulse [27]. For a 10 ns laser pulse with peak intensity $I_0 = 7 \times 10^{11} \text{ W/cm}^2$ and a weak dc field, $E_s = 286 \text{ V/cm}$, tilted with respect to each other an angle $\beta = 135^\circ$, the experimentally measured degree of orientation was $N_{\text{up}}/N_{\text{tot}} = 0.71$ [1]. For this field configuration, we perform a theoretical study including 54 rotational states of the state-selected molecular beam of this experiment, i. e., accounting for 92.5% of the total population in the beam [1].

The adiabatic approximation, which assumes that the field-dressed instantaneous eigenstate is a solution of the time-dependent Hamiltonian, would give rise to a very weakly oriented ensemble with $N_{\text{up}}/N_{\text{tot}} = 0.55$ [2]. This result is in contradiction with the experimental observation and indicates that the mixed-field orientation is, in general, a non adiabatic process [2]. The weak electric field is responsible for breaking the azimuthal symmetry, and for coupling states with different field-free magnetic quantum numbers. Based on this fact, we had proposed a diabatic model [2], which improves the adiabatic description by classifying the avoided crossings: as $I(t)$ increases, they are crossed diabatically (adiabatically) if the involved states have different (same) field-free expectation value $\langle M^2 \rangle$. The diabatic model is equivalent to an adiabatic description of a parallel field configuration including only the dc electric field component parallel to the alignment laser field $E_s \cos \beta$, and neglecting the perpendicular component. Within this diabatic model, the orientation ratio of the state-selected molecular beam is $N_{\text{up}}/N_{\text{tot}} = 0.624$, which is larger than for the pure adiabatic description, but still smaller than the experimental measurement.

To check the validity of the diabatic model, we have solved the time-dependent Schrödinger equation considering a dc field parallel to the LFF Z -axis with strength $E_s \cos \beta$. Hence, the field-dressed rotational dynamics takes into account the non-adiabatic couplings between states with the same magnetic quantum number and the pendular doublets formation [33]. In this description, we obtain a smaller orientation ratio $N_{\text{up}}/N_{\text{tot}} = 0.623$ than the experimentally measured. For a full non-adiabatic description, we have taken into account all the couplings, and, in particular, those between states with different field-free magnetic quantum numbers, which were neglected in the parallel-field time-dependent description, and solved the time-dependent Schrödinger equation associated to Hamiltonian (1) for each initially populated state. The obtained degree of orientation $N_{\text{up}}/N_{\text{tot}} = 0.612$ is still lower than the experimental one, and even lower than the simplified models described above. The discrepancies between the time-dependent descriptions of the tilted and parallel fields configurations arise due to the couplings between the states within the $|J_{K_a, K_c} M\rangle$ -manifold with $0 \leq M \leq J$, i. e., degenerate states in the field-free case, which differ in the magnetic quantum number M , at weak laser intensities, i. e., $I \lesssim 1 \times 10^{18} \text{ W/cm}^2$, and between the states with different field-free magnetic quantum numbers at strong intensities [30].

To analyze these theoretical results, we build up the molecular ensemble by successively adding states according to their populations in the experimental state-selected beam. The orientation ratio $N_{\text{up}}/N_{\text{tot}}$ is plotted in Fig. 1 versus the percentage of population included in the experimental molecular beam. For the ground state, which has the largest population, we obtain $\langle \cos\theta \rangle = 0.986$ and $N_{\text{up}}/N_{\text{tot}} = 0.999$, which is very

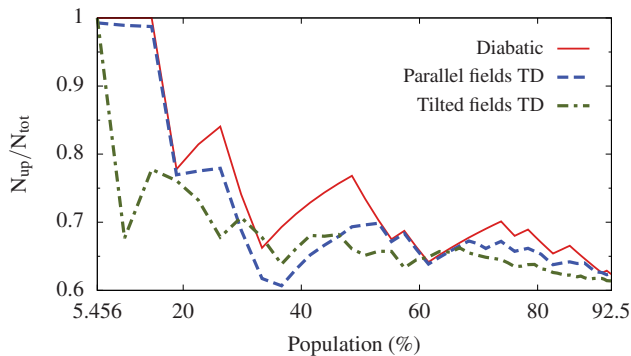


FIG. 1. The theoretical orientation ratio $N_{\text{up}}/N_{\text{tot}}$ as a function of the population of the molecular beam of benzonitrile using a probe laser circularly polarized perpendicular to the screen computed by the diabatic model (red solid line), by time-dependent (TD) description for parallel-fields (blue dashed line) and time-dependent description for tilted-fields (green dot-dashed line). The field configuration is $I_0 = 7 \times 10^{11} \text{ W/cm}^2$, $E_s = 286 \text{ V/cm}$ and $\beta = 135^\circ$.

close to the adiabatic result $N_{\text{up}}/N_{\text{tot}} = 1$. As more states are included in the ensemble, the orientation ratio $N_{\text{up}}/N_{\text{tot}}$ decreases with a superimposed oscillatory behavior due to the orientation or antiorientation of the additionally included states. The discrepancies between these results illustrate the importance of performing a full time-dependent description of the mixed field orientation process.

Several reasons could explain the disagreement between the time-dependent study and the experimental result. First, we do not include the finite spatial profile of the alignment and probe lasers which implies that all the molecules in the beam do not feel the same laser intensity. Based on our previous studies [2], we can conclude that this effect should not significantly modify the degree of orientation. Second, it has been assumed that the state selection along the dc-field deflector is an adiabatic process [3, 4, 27], if this would not be the case, the rotational states before the mixed-field orientation experiment would not be pure field-free states. Third, the mixed-field dynamics is very sensitive to the field configuration, and small variations on it, e.g., on the pulse shape, could significantly affect these results. Finally, by adding the rest of states forming the experimental molecular beam, the theoretical degree of orientation will not approach to the experimental one. Assuming that the rest of the states are not oriented, or that half of them are fully oriented and the other half fully antioriented, the theoretical degree of orientation would be reduced to 0.605, still far from the experimental value.

The adiabatic and diabatic approximations predict pendular states either fully oriented $N_{\text{up}}/N_{\text{tot}} \approx 1$ or antioriented $N_{\text{up}}/N_{\text{tot}} \approx 0$, whereas in a time-dependent description they are not fully oriented or fully antioriented with $0 \lesssim N_{\text{up}}/N_{\text{tot}} \lesssim 1$. This is illustrated in Fig. 2 with the 2D projection of the probability den-

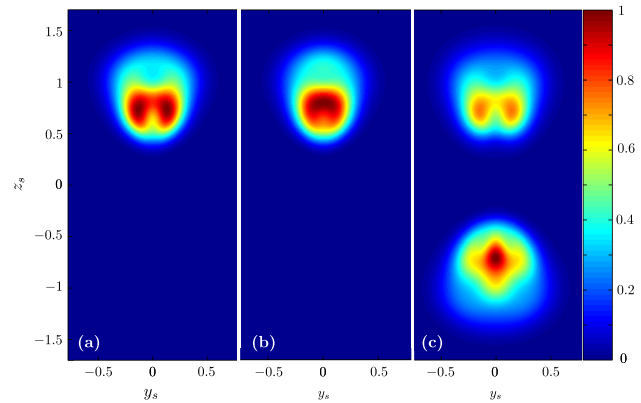


FIG. 2. The 2D projection of the probability density of the state $|3_{0,3}1\rangle_t$ at the peak intensity computed using (a) the adiabatic approximation, (b) the diabatic model, and (c) the time-dependent description for tilted fields. The field configuration is $I_0 = 7 \times 10^{11} \text{ W/cm}^2$, $E_s = 286 \text{ V/cm}$ and $\beta = 135^\circ$.

sity of the $|3_{0,3}1\rangle_t$ state at the peak intensity. For the adiabatic and diabatic descriptions, the 2D probability density is concentrated on the upper part of the screen with $N_{\text{up}}/N_{\text{tot}} = 1$. In contrast, the time-dependent description provides a weakly antioriented state with $N_{\text{up}}/N_{\text{tot}} \approx 0.44$, see Fig. 2 (c). This is due to the contributions of antioriented pendular states to the rotational dynamics: at the peak intensity the antioriented adiabatic pendular state $|2_{2,0}1\rangle_p$ has the largest contribution with a weight of 41.1% into the $|3_{0,3}1\rangle_t$ time-dependent wave function.

IV. FIELD-DRESSED DYNAMICS OF A ROTATIONAL EXCITED STATE

The rotational dynamics in tilted fields is more complex than in parallel fields [33]. We illustrate this complexity by analyzing the field-dressed dynamics of the excited state $|3_{0,3}1\rangle$, which has been studied for parallel fields in Ref. [33]. For tilted fields, the adiabatic pendular state $|3_{0,3}1\rangle_p$ is the ninth one of the even-even irreducible representation, and is oriented in a strong laser field combined with a weak static electric field.

In Fig. 3 we plot the orientation $\langle \cos \theta \rangle$ of the state $|3_{0,3}1\rangle_t$ as a function of the laser intensity $I(t)$ for three different field configurations (a) $\beta = 0^\circ$, (b) $\beta = 30^\circ$ and (c) $\beta = 60^\circ$, with $E_s = 300 \text{ V/cm}$, and laser pulses with temporal widths $\tau = 0.5 \text{ ns}$, 1 ns , 5 ns and 10 ns and peak intensity $I_0 = 7 \times 10^{11} \text{ W/cm}^2$. For these field configurations, the adiabatic orientation is given by $\langle \cos \theta \rangle = 0.97$, and weakly affected by the inclination angle of the dc-field β .

For parallel fields, $|3_{0,3}1\rangle_p$ is the third adiabatic state in the irreducible representation with $M = 1$ and even parity under two-fold rotations around the MFF z -axis. This state is oriented in the pendular regime. As $I(t)$ in-

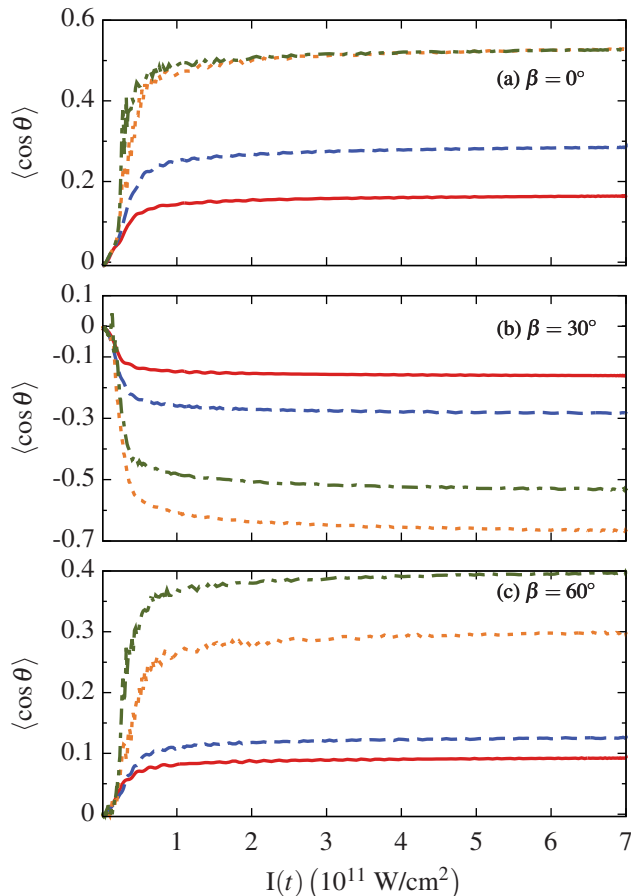


FIG. 3. For the $|3_{0,3}1\rangle_t$ state, expectation value $\langle \cos \theta \rangle$ as a function of $I(t)$ for laser pulses with peak intensity $I_0 = 7 \times 10^{11}$ W/cm 2 and temporal widths $\tau = 0.5$ (red solid), 1 (blue dashed), 5 (orange dotted) and 10 ns (green dot-dashed). The electric field has strength $E_s = 300$ V/cm, and is tilted an angle (a) $\beta = 0^\circ$, (b) $\beta = 30^\circ$ and (c) $\beta = 60^\circ$.

creases, the orientation shows an increasing trend with a superimposed smooth oscillatory behavior, which is due to the couplings among the adiabatic pendular states contributing to the non-adiabatic dynamics. Three adiabatic pendular states, $|3_{0,3}1\rangle_p$ (oriented), $|2_{2,1}1\rangle_p$ (antioriented), and $|2_{2,0}1\rangle_p$ (oriented), dominantly contribute to the time-dependent wave function of $|3_{0,3}1\rangle_t$. The coupling between the oriented adiabatic pendular states, i. e., $|3_{0,3}1\rangle_p$ and $|2_{2,0}1\rangle_p$, provokes the oscillations, because in the pendular regime their couplings with the antioriented one are close to zero, i. e., ${}_p\langle 3_{0,3}1 | \cos \theta | 2_{2,1}1 \rangle_p \approx 0$ and ${}_p\langle 2_{2,0}1 | \cos \theta | 2_{2,1}1 \rangle_p \approx 0$ [33]. The contribution of the antioriented adiabatic pendular state reduces the degree of orientation compared to the adiabatic prediction. As the temporal width of the pulse τ increases, the dynamics becomes more adiabatic and the orientation increases approaching to the adiabatic limit.

Due to the splitting of the field-free degenerate $|3_{0,3}M\rangle$ -multiplet in tilted fields, the adiabatic pendular states $|3_{0,3}M\rangle_p$, with $M = 0, 1, 2, 3$, contribute to the

field-dressed dynamics of $|3_{0,3}1\rangle_t$ and their weights depend on the angle β and on the dc-field strength. For $\beta = 30^\circ$, the $|3_{0,3}1\rangle_t$ wave function is antioriented, which can be rationalized in terms of the adiabatic pendular states contributing to the rotational dynamics. Once the multiplet is split, the contribution of the adiabatic pendular states $|3_{0,3}M\rangle_p$ onto the $|3_{0,3}1\rangle_t$ wave function is approximately the same for all the pulses. From this moment on, the way the laser is turned on plays an important role on the dynamics. We find up to 27 adiabatic pendular states with $J \leq 4$ contributing to the dynamics of $|3_{0,3}1\rangle_t$, and the antioriented adiabatic pendular state $|2_{2,0}1\rangle_p$ has the largest contribution to the time-dependent wave function, larger than 67% for $\tau = 5$ ns and 10 ns. By decreasing the temporal width of the pulse, more adiabatic pendular states contribute to the dynamics, and $|\langle \cos \theta \rangle|$ diminishes because the weights of oriented and antioriented adiabatic states are very similar. In contrast, $|3_{0,3}1\rangle_t$ is oriented if the dc-field is tilted an angle $\beta = 60^\circ$. For this case, the dominant contributions to the wave function are due to the $|2_{2,1}2\rangle_p$ and $|3_{2,1}3\rangle_p$ oriented states for $\tau = 10$ ns and $\tau = 5$ ns, and to $|3_{2,1}3\rangle_p$ for $\tau = 1$ ns and $\tau = 0.5$ ns. As τ increases, the orientation increases, but it is smaller than the adiabatic limit of the orientation $\langle \cos \theta \rangle = 0.97$.

The dc-field strength determines the energy gap between the two states forming a pendular doublet in the strong laser field regime. Thus, by increasing the dc-field strength the dynamics should become more adiabatic because the population transferred between these two states as the pendular doublet is formed should be reduced. For a 10 ns alignment pulse, we present in Fig. 4 the orientation of the $|3_{0,3}1\rangle_t$ state versus the laser intensity $I(t)$ for dc-fields strengths $E_s = 5$ kV/cm, $E_s = 10$ kV/cm and $E_s = 20$ kV/cm. Let us remark that for strong dc fields, the energy gap between two states forming the pendular doublets in a strong ac field is large and they are not quasidegenerate, and, in particular, the interaction due to the static electric field could not be treated as a perturbation to the ac-field interaction. Even for these strong electric fields, the rotational dynamics is non-adiabatic, and this state is either weakly oriented, strongly oriented or antioriented depending on the field configuration, see Fig. 4. This can be explained in terms the splitting of the $|3_{0,3}M\rangle_p$ manifold and of the avoided crossings that are encountered during the time evolution of the wave packet, which, in most cases, are not crossed adiabatically [33]. For strong dc fields, the avoided crossings between adiabatic pendular states evolving from different multiplets become more likely. For $E_s = 20$ kV/cm, the orientation at the peak intensity is very similar for the three tilted angles, which is due to the dominant contribution of oriented adiabatic pendular states to the rotational dynamics.

For the $|3_{0,3}1\rangle_t$ state, we compare in Fig. 5 the orientation in tilted fields with the results obtained in a parallel field configuration which includes only the Z -

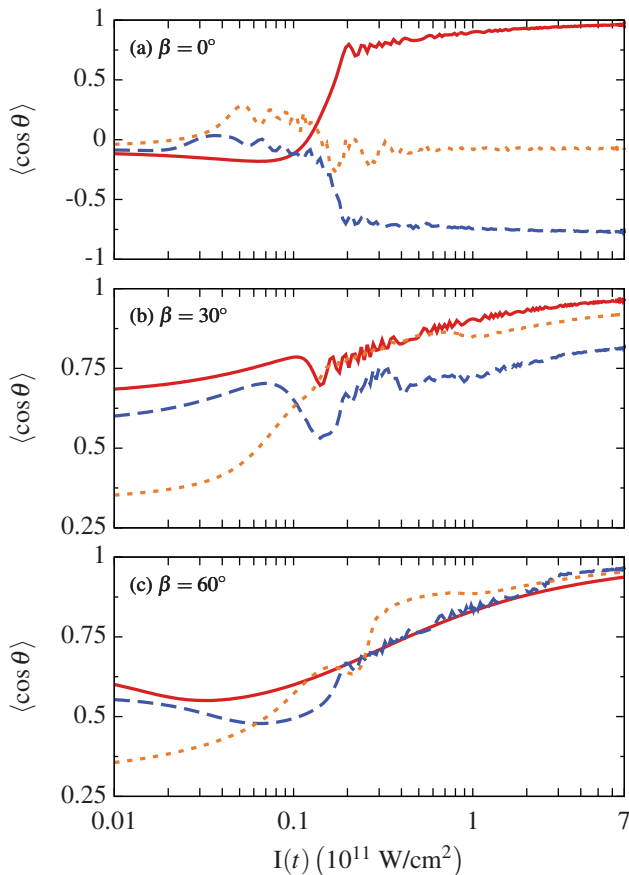


FIG. 4. For the $|3_{0,31}\rangle_t$ state, expectation value $\langle \cos \theta \rangle$ as a function of $I(t)$ for a 10 ns laser pulse with peak intensity $I_0 = 7 \times 10^{11}$ W/cm 2 . The electric field has strengths (a) $E_s = 5$ kV/cm, (b) $E_s = 10$ kV/cm, and (c) $E_s = 20$ kV/cm, and is tilted by $\beta = 0^\circ$ (red solid), $\beta = 30^\circ$ (blue dashed) and $\beta = 60^\circ$ (orange dotted).

component of the electric field $E_s \cos \beta$. For this parallel field configuration, the state is oriented, $\langle \cos \theta \rangle$ increases as E_s is enhanced and shows a plateau like behavior for $I(t) \gtrsim 1 \times 10^{11}$ W/cm 2 . In contrast, for tilted-fields, the $|3_{0,31}\rangle_t$ state is anti-oriented for weak dc-fields $E_s = 300$ V/cm and $E_s = 1$ kV/cm, and oriented for $E_s = 10$ kV/cm and $E_s = 20$ kV/cm. The discrepancy between these results illustrates the importance of the dc-field perpendicular to the non-resonant laser. The non-adiabatic phenomena that take place for tilted fields, i. e., the splitting of the $|3_{0,3M}\rangle_p$ manifold and the avoided crossing among pendular states having different field-free magnetic quantum number, strongly affect the field-dressed dynamics. For weak electric fields, the impact of these non-adiabatic effects is larger and the direction of the orientation is reversed. Whereas, for strong dc fields, they show qualitatively similar but quantitative different orientation.

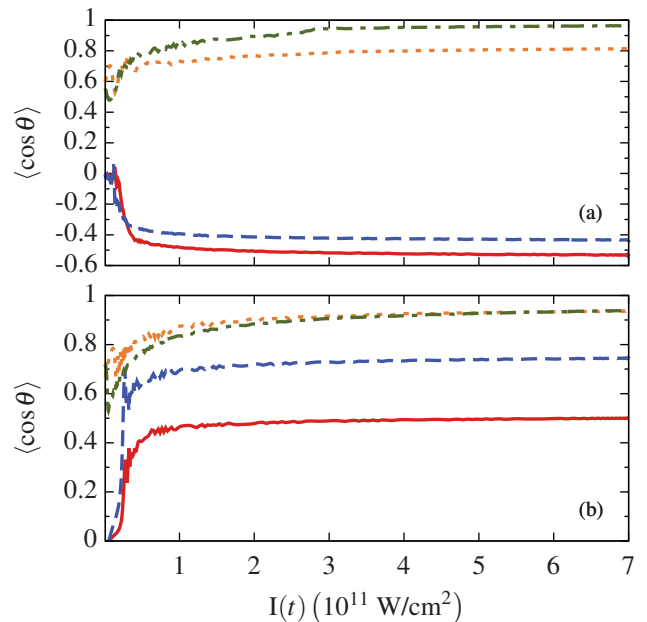


FIG. 5. For the $|3_{0,31}\rangle_t$ state, expectation value $\langle \cos \theta \rangle$ as a function of $I(t)$ for a 10 ns laser pulse with peak intensity $I_0 = 7 \times 10^{11}$ W/cm 2 for (a) tilted fields with $\beta = 30^\circ$ and for (b) parallel fields with the electric field parallel to the LFF Z-axis of strength $E_s \cos 30^\circ$. The electric field strengths are $E_s = 300$ V/cm (red solid line), $E_s = 1$ kV/cm (blue dashed line), $E_s = 10$ kV/cm (orange dotted-line), and $E_s = 20$ kV/cm (green dot-dashed line)

V. SOURCES OF NON-ADIABATIC EFFECTS

For tilted fields, the dynamics is characterized by the pendular doublet formation, the splitting of the degenerate $|J_{K_a, K_c} M\rangle$ -multiplet at weak laser intensities, and a large amount of avoided crossings, some of them due to the tilted electric field which breaks the azimuthal symmetry. Since the formation of the pendular doublet has been discussed in detail in our work on asymmetric top molecules in parallel fields [33], we focus here on exploring the other two non-adiabatic phenomena.

Let us mention that the rotational dynamics of the ground state of each irreducible representation is only affected by the pendular doublet formation, as the absolute ground state. Thus, for them, it is easy to reach the adiabatic mixed-field orientation limit [33].

A. Coupling in the J -manifold

In the field-free case, the $|J_{K_a, K_c} M\rangle$ states with $0 \leq M \leq J$ are degenerate due to the azimuthal symmetry. The weak electric field of the mixed-field orientation experiments breaks their M -degeneracy by the quadratic Stark splitting, $\Delta E \sim E_s^2$. For $E_s = 300$ V/cm and $\beta = 30^\circ$, the neighboring levels of the $|3_{0,3M}\rangle$ -manifold are separated by 1.6×10^{-4} cm $^{-1}$, 9.4×10^{-5} cm $^{-1}$

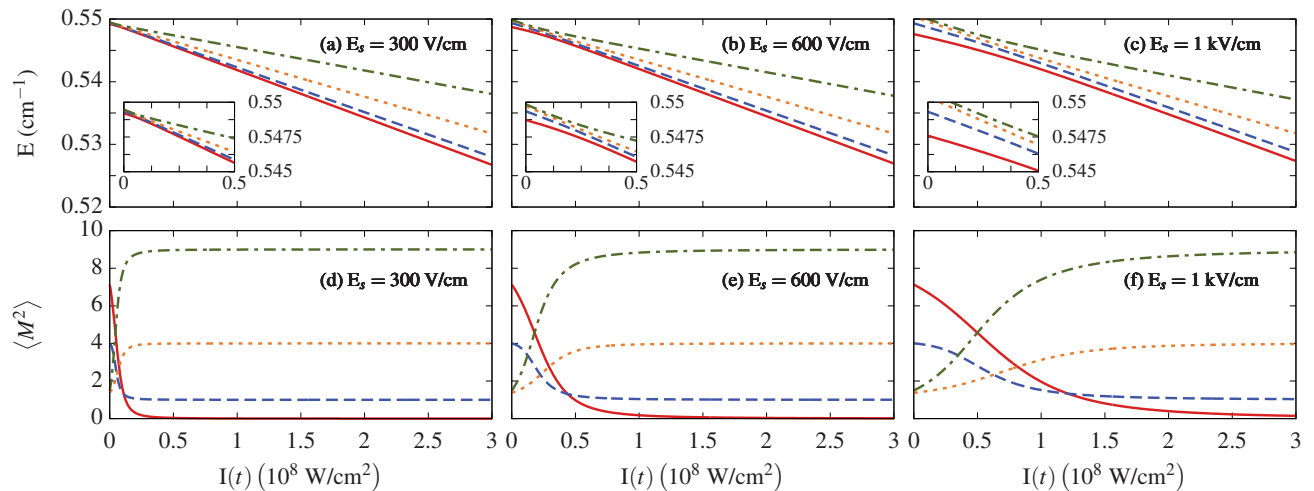


FIG. 6. For the adiabatic pendular states $|3_{0,31}\rangle_t$ (black double-dot-dashed line), $|3_{0,33}\rangle_p$ (red solid line), $|3_{0,32}\rangle_p$ (blue dashed), $|3_{0,31}\rangle_p$ (orange dotted line) and $|3_{0,30}\rangle_p$ (green dot-dashed), energy and expectation value $\langle M^2 \rangle$ for a dc field tilted $\beta = 30^\circ$ and with strength $E_s = 300$ V/cm (a) and (d), $E_s = 600$ V/cm (b) and (e), and $E_s = 1000$ V/cm (c) and (f). The laser pulse has $\tau = 10$ ns and peak intensity $I_0 = 7 \times 10^{11}$ W/cm 2 .

and 3.1×10^{-5} cm $^{-1}$. Due to these small energy gaps, even a weak laser field provokes strong couplings among them, which significantly affect the rotational dynamics. We consider a dc field tilted $\beta = 30^\circ$ with strengths $E_s = 300$ V/cm, 600 V/cm, and 1000 V/cm. In Fig. 6 we present the energy, and expectation value $\langle M^2 \rangle$ of the adiabatic pendular states $|3_{0,3M}\rangle_p$ as the laser intensity is increased till $I(t) = 3 \times 10^8$ W/cm 2 . In the presence of only an electric field forming an angle β with the LFF Z -axis, the projection of \mathbf{J} along the dc-field axis is a good quantum number, but not along the LFF Z -axis, cf. Fig. 6 (d), (e), and (f). As the laser intensity increases, the levels suffer several avoided crossings, whose widths are larger for stronger dc-fields, see Fig. 6 (a)-(c). The effects of these avoided crossings are recognized in the time evolution of $\langle M^2 \rangle$. After them, $\langle M^2 \rangle$ shows a constant behavior as $I(t)$ is increased. Indeed, when the interaction due to the laser field is dominant, the projection of \mathbf{J} along the LFF Z -axis becomes a quasi good quantum number, as is observed in Fig. 6 (d), (e) and (f).

The couplings within the states of the $|J_{K_a, K_c} M\rangle_p$ -manifold have a strong impact on the rotational dynamics since, for a given state, the time-dependent wave function might have contributions from all the adiabatic pendular states within this multiplet. This is illustrated in Fig. 7 with the weights of the adiabatic pendular states $|3_{0,3M}\rangle_p$ into the time-dependent wave function of $|3_{0,31}\rangle_t$ for $E_s = 300$ V/cm, 600 V/cm and 1000 V/cm, $\beta = 30^\circ$ and a 10 ns laser pulse with peak intensity $I_0 = 7 \times 10^{11}$ W/cm 2 . As $I(t)$ increases, the weights of the adiabatic pendular states change drastically and are redistributed within the manifold. This population transfer depends on the coupling among the states in the multiplet, on the initial energy gap between them, which

is determined by the dc-field strength and the angle β , and on the way the alignment pulse is turned on. The field-dressed dynamics in this region is characterized by large time scales and very large adiabaticity ratios $\eta \gg 1$ among the adiabatic pendular states [30]. As a consequence, very long laser pulses are required to reach the adiabatic limit. Once the manifold is split, the weights reach a plateau-like behavior, which is kept till one of the adiabatic pendular states suffers an avoided crossing, which might occur at stronger laser intensities.

B. Check of the diabatic model

In this section, we check the validity of the diabatic model, which is based on the weak coupling, induced by the tilted weak electric field, between states with different field-free magnetic quantum numbers [2]. In the presence of only a laser field, the magnetic quantum number of the field-dressed states is conserved, and by adding a tilted static electric field the rotational symmetry around the laser polarization axis of the ac-field Hamiltonian is broken. For a weak dc field, the interaction due to this dc field could be considered as a perturbation to the ac-field Hamiltonian, and, in this case, $\langle M^2 \rangle$ is almost conserved. The diabatic model assumes that an avoided crossing is crossed adiabatically (diabatically) if the two involved states have the same (different) $\langle M^2 \rangle$. Then, the adiabatic model implies that $\langle M^2 \rangle$ should approximately remain constant.

As an example, we present in Fig. 8 the time evolution of $\langle M^2 \rangle$ for the $|3_{0,31}\rangle_t$ state in several field configurations. Before the pulse is turned on, the initial state is the adiabatic pendular level of the corresponding dc-field configuration, and, as indicated above, $\langle M^2 \rangle$ differs

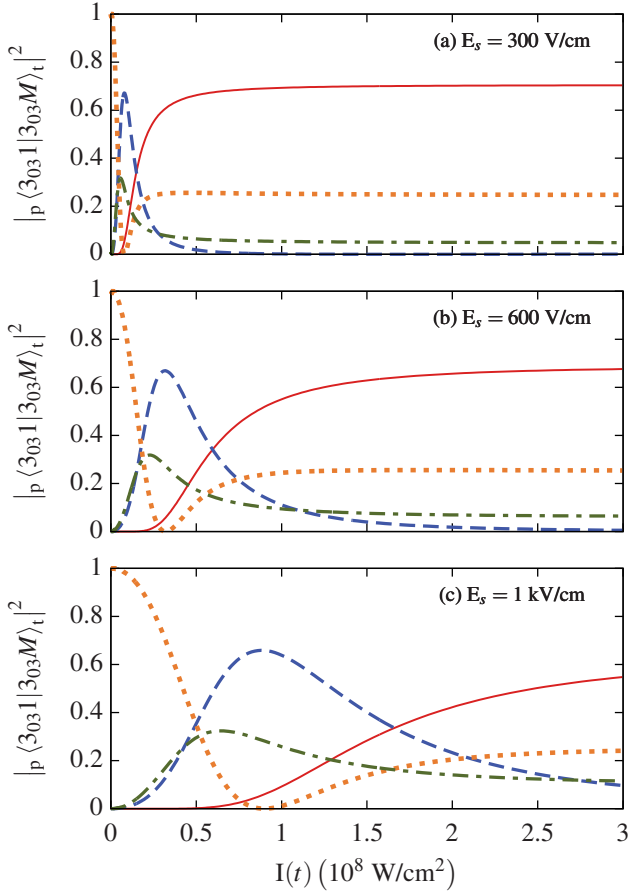


FIG. 7. The squares of the projection of the time-dependent wave function $|3_{0,3}1\rangle_t$ onto the adiabatic states of the $|3_{0,3}M\rangle$ multiplet, i.e., $|3_{0,3}3\rangle_p$, $|3_{0,3}2\rangle_p$, $|3_{0,3}1\rangle_p$ and $|3_{0,3}0\rangle_p$ as a function of $I(t)$. The field configurations are $I_0 = 7 \times 10^{11} \text{ W/cm}^2$, $\tau = 10 \text{ ns}$, $\beta = 30^\circ$ and (a) $E_s = 300 \text{ V/cm}$, (b) $E_s = 600 \text{ V/cm}$, and (c) $E_s = 1000 \text{ V/cm}$. The labels of the states are the same as in Fig. 6.

from its field-free value due to the tilted electric field. As $I(t)$ increases, $\langle M^2 \rangle$ increases and reaches a maximum, which appears at lower intensities for longer pulses. If the pulse is short, the rotational dynamics does not adapt to the time-dependent interaction, which provokes non-adiabatic avoided crossings, and $\langle M^2 \rangle$ does not change significantly. For longer pulses, the field-dressed dynamics is more adiabatic and larger changes on $\langle M^2 \rangle$ are observed at moderate laser intensities, and, therefore, $\langle M^2 \rangle$ reaches a larger value at the maximum. By increasing the dc-field strength, the Stark couplings among neighboring levels are larger provoking larger changes in $\langle M^2 \rangle$, see Fig. 8(a) and (c). After the first maximum, $\langle M^2 \rangle$ shows a rapid oscillatory behavior due to the presence of several avoided crossings, which are crossed diabatically transferring part of the population. For $\tau = 10 \text{ ns}$, $E_s = 300 \text{ V/cm}$, $\beta = 30^\circ$ and $\beta = 60^\circ$, $\langle M^2 \rangle$ shows a sudden change due to highly non-adiabatic avoided crossing among states with different values of $\langle M^2 \rangle$. For

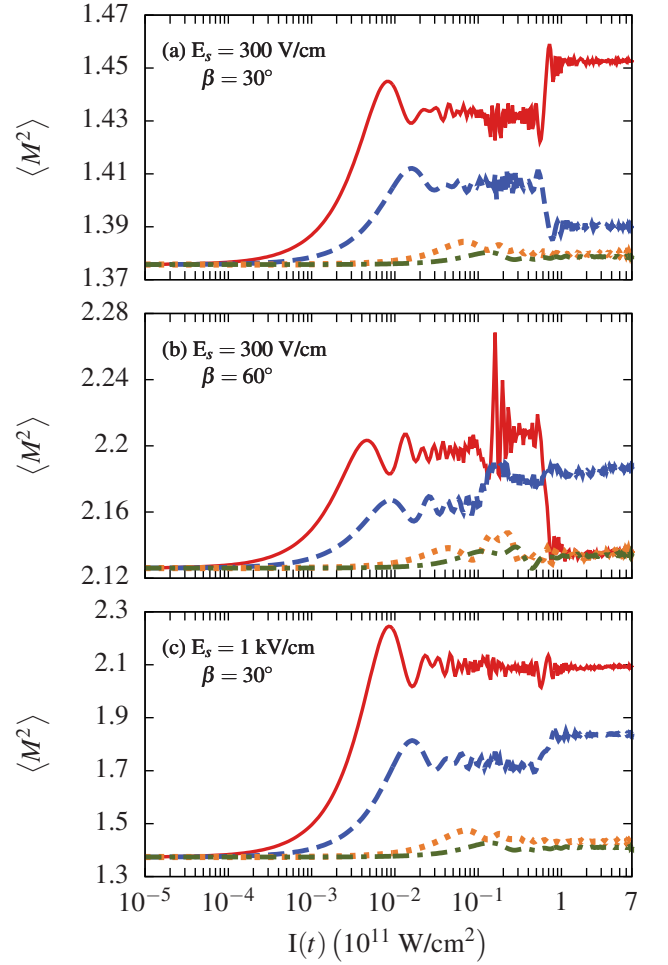


FIG. 8. For the time-dependent state $|3_{0,3}1\rangle_t$, expectation $\langle M^2 \rangle$ as a function of $I(t)$ for the rotational state for (a) $E_s = 300 \text{ V/cm}$ and $\beta = 30^\circ$ (b) $E_s = 300 \text{ V/cm}$ and $\beta = 60^\circ$ and (c) $E_s = 1000 \text{ V/cm}$ and $\beta = 30^\circ$. The laser pulse has $I_0 = 7 \times 10^{11} \text{ W/cm}^2$, and temporal widths $\tau = 10 \text{ ns}$ (red solid line), 5 ns (blue dashed line), 1 ns (orange dotted line) and 0.5 ns (green dot-dashed line).

$I(t) \gtrsim 10^{11} \text{ W/cm}^2$, $\langle M^2 \rangle$ reaches a plateau-like behavior with small fluctuations, and, therefore, in this region the diabatic model provides a good approximation to the field-dressed dynamics.

These results show that the failure of the diabatic model mainly occurs at low or moderate laser field intensities. In this regime, the field dressed states are strongly coupled and several non-adiabatic effects take place resulting on a time-dependent wave function which is a linear combination of the eigenstates of the instantaneous field-dressed Hamiltonian. These non-adiabatic effects cannot be captured by the diabatic model, since it considers an unambiguous correspondence between eigenstates.

VI. CONCLUSIONS

In this work, we have investigated the rotational dynamics of asymmetric-top molecules on a tilted-field configuration similar to those used in current mixed-field orientation experiments. By considering the benzonitrile molecule as prototype, the richness and variety of the field-dressed dynamics have been illustrated. We have addressed unique non-adiabatic effects of the tilted field configuration such as the J -multiplet splitting and the coupling between states with different field-free magnetic quantum numbers. By increasing the dc-field strength, the energy spacings among the states on a J -manifold and on the quasidegenerate pendular doublets are enhanced. Thus, the characteristic time scales of these two non-adiabatic phenomena are reduced easing the experimental requirements for an adiabatic dynamics. However, the large amount of narrow avoided crossings that emerge for moderate and strong laser intensities frustrates the hunt of an adiabatic field-dressed dynamics for rotationally excited states. As a consequence, for excited rotational states, it becomes more challenging to experimentally reach the adiabatic limit.

In this time-dependent framework, we have revisited the mixed-field orientation experiment of a state-selected molecular beam of benzonitrile [1]. Our analysis includes 92.5% of the molecular beam with the experimental weights, and the experimental field configuration: a weak static electric field combined with a non-resonant linearly polarized laser pulses. In this time-dependent description, the degree of orientation of the molecular ensemble is smaller than the experimentally measured [1]

and similar to the orientation provided by the diabatic model [2]. By completing the molecular beam with the rest of populated states in the experiment and taking into account the volume effect, this time-dependent orientation ratio should not be significantly modified and should not become closer to the experimental one. The disagreement between the theoretical and experimental results could be due to the Coulomb explosion, and the subsequent detection of the molecular ions, and the way these processes are simulated or to the lack of adiabaticity on previous steps of the experiment, such as the state selection, which might modify the experimental weights of the rotational states in the molecular beam.

A rather natural extension of this work would be to investigate the rotational dynamics of an asymmetric-top molecule without rotational symmetry. This time-dependent study should allow us to review the conclusions of the adiabatic analysis of the 6-chloropyridazine-3-carbonitrile (CPC) in combined electric and non-resonant laser fields [42].

ACKNOWLEDGMENTS

We would like to thank Jochen Küpper, Henrik Stapelfeldt, and Linda V. Thesing for fruitful discussions, and Hans-Dieter Meyer for providing us the code of the short iterative Lanczos algorithm. Financial support by the Spanish project FIS2014-54497-P (MINECO), and the Andalusian research group FQM-207 is gratefully appreciated. JJO acknowledges the support by the Vilum Kann Rasmussen (VKR) Center of Excellence QUSCOPE.

-
- [1] J. L. Hansen, L. Holmegaard, L. Kalhøj, S. L. Kragh, H. Stapelfeldt, F. Filsinger, G. Meijer, J. Küpper, D. Dimitrovski, M. Abu-samha, C. P. J. Martiny, and L. B. Madsen, *Phys. Rev. A* **83**, 023406 (2011).
- [2] J. J. Omiste, M. Gärtner, P. Schmelcher, R. González-Férez, L. Holmegaard, J. H. Nielsen, H. Stapelfeldt, and J. Küpper, *Phys. Chem. Chem. Phys.* **13**, 18815 (2011).
- [3] L. Holmegaard, J. H. Nielsen, I. Nevo, H. Stapelfeldt, F. Filsinger, J. Küpper, and G. Meijer, *Phys. Rev. Lett.* **102**, 023001 (2009).
- [4] I. Nevo, L. Holmegaard, J. Nielsen, J. L. Hansen, H. Stapelfeldt, F. Filsinger, G. Meijer, and J. Küpper, *Phys. Chem. Chem. Phys.* **11**, 9912 (2009).
- [5] E. Frumker, C. T. Hebeisen, N. Kajumba, J. B. Bertrand, H. J. Wörner, M. Spanner, D. M. Villeneuve, A. Naumov, and P. B. Corkum, *Phys. Rev. Lett.* **109**, 113901 (2012).
- [6] S. Trippel, T. Mullins, N. L. M. Müller, J. S. Kienitz, K. Długolecki, and J. Küpper, *Mol. Phys.* **111**, 1738 (2013).
- [7] J. H. Mun, D. Takei, S. Minemoto, and H. Sakai, *Phys. Rev. A* **89**, 051402 (2014).
- [8] P. M. Kraus, D. Baykusheva, and H. J. Wörner, *J. Phys. B: At. Mol. Opt.* **47**, 124030 (2014).
- [9] P. Peng, N. Li, J. Li, H. Yang, P. Liu, R. Li, and Z. Xu, *Opt. Lett.* **38**, 4872 (2013).
- [10] B. Zhang, S. Yu, Y. Chen, X. Jiang, and X. Sun, *Phys. Rev. A* **92**, 053833 (2015).
- [11] Y. P. Li, S. J. Yu, X. Y. Duan, Y. Z. Shi, and Y. J. Chen, *J. Phys. B At. Mol. Opt. Phys.* **49**, 075603 (2016).
- [12] H. J. Loesch and J. Möller, *J. Chem. Phys.* **97**, 9016 (1992).
- [13] T. P. Rakitzis, A. J. van den Brom, and M. H. M. Janssen, *Science* **303**, 1852 (2004).
- [14] S. Ospelkaus, K.-K. Ni, D. Wang, M. H. G. de Miranda, B. Neyenhuis, G. Quémener, P. S. Julienne, J. L. Bohn, D. S. Jin, and J. Ye, *Science* **327**, 853 (2010).
- [15] G. Quémener and J. L. Bohn, *Phys. Rev. A* **81**, 060701 (2010).
- [16] H. J. Loesch and A. Remscheid, *J. Chem. Phys.* **93**, 4779 (1990).
- [17] K.-K. Ni, S. Ospelkaus, D. Wang, G. Quémener, B. Neyenhuis, M. H. G. de Miranda, J. L. Bohn, J. Ye, and D. S. Jin, *Nature* **464**, 1324 (2010), 1001.2809.
- [18] A. B. Henson, S. Gersten, Y. Shagam, J. Narevicius, and E. Narevicius, *Science* **338**, 234 (2012).
- [19] S. N. Vogels, J. Onvlee, S. Chefdeville, A. van der Avoird,

- G. C. Groenenboom, and S. Y. T. van de Meerakker, *Science* **350**, 787 (2015).
- [20] M. Yamazaki, K. Oishi, H. Nakazawa, C. Zhu, and M. Takahashi, *Phys. Rev. Lett.* **114**, 103005 (2015).
- [21] T. Kierspel, J. Wiese, T. Mullins, J. Robinson, A. Aquila, A. Barty, R. Bean, R. Boll, S. Boutet, P. Bucksbaum, H. N. Chapman, L. Christensen, A. Fry, M. Hunter, J. E. Koglin, M. Liang, V. Mariani, A. Morgan, A. Natan, V. Petrovic, D. Rolles, A. Rudenko, K. Schnorr, H. Stapelfeldt, S. Stern, J. Thøgersen, C. H. Yoon, F. Wang, S. Trippel, and J. Küpper, *J. Phys. B At. Mol. Opt. Phys.* **48**, 204002 (2015), 1506.03650.
- [22] B. Friedrich and R. Herschbach, *J. Phys. Chem. A* **103**, 10280 (1999).
- [23] B. Friedrich and D. R. Herschbach, *J. Chem. Phys.* **111**, 6157 (1999).
- [24] R. Baumfalk, N. H. Nahler, and U. Buck, *J. Chem. Phys.* **114**, 4755 (2001).
- [25] H. Sakai, S. Minemoto, H. Nanjo, H. Tanji, and T. Suzuki, *Phys. Rev. Lett.* **90**, 083001 (2003).
- [26] H. Tanji, S. Minemoto, and H. Sakai, *Phys. Rev. A* **72**, 063401 (2005).
- [27] F. Filsinger, J. Küpper, G. Meijer, L. Holmegaard, J. H. Nielsen, I. Nevo, J. L. Hansen, and H. Stapelfeldt, *J. Chem. Phys.* **131**, 064309 (2009).
- [28] O. Ghafur, A. Rouzee, A. Gijsbertsen, W. K. Siu, S. Stolte, and M. J. J. Vrakking, *Nat Phys* **5**, 289 (2009).
- [29] J. H. Nielsen, H. Stapelfeldt, J. Küpper, B. Friedrich, J. J. Omiste, and R. González-Férez, *Phys. Rev. Lett.* **108**, 193001 (2012).
- [30] J. J. Omiste and R. González-Férez, *Phys. Rev. A* **86**, 043437 (2012).
- [31] J. S. Kienitz, S. Trippel, T. Mullins, K. Długołęcki, R. González-Férez, and J. Küpper, *ChemPhysChem* 10.1002/cphc.201600710.
- [32] S. Trippel, T. Mullins, N. L. M. Müller, J. S. Kienitz, R. González-Férez, and J. Küpper, *Phys. Rev. Lett.* **114**, 103003 (2015).
- [33] J. J. Omiste and R. González-Férez, *Phys. Rev. A* **88**, 033416 (2013).
- [34] L. Holmegaard, J. L. Hansen, L. Kalhøj, S. L. Kragh, H. Stapelfeldt, F. Filsinger, J. Küpper, G. Meijer, D. Dimitrovski, M. Abu-samha, C. P. J. Martiny, and L. B. Madsen, *Nat. Phys.* **6**, 428 (2010).
- [35] R. N. Zare, *Angular Momentum: Understanding Spatial Aspects in Chemistry and Physics* (John Wiley and Sons, New York, 1988).
- [36] K. Wohlfart, M. Schnell, J.-U. Grabow, and J. Küpper, *J. Mol. Spectrosc* **247**, 119 (2007).
- [37] T. Seideman and E. Hamilton, *Adv. Atom. Mol. Opt. Phys.* **52**, 289 (2006).
- [38] J. J. Omiste, R. González-Férez, and P. Schmelcher, *J. Chem. Phys.* **135**, 064310 (2011).
- [39] M. Beck, A. Jäckle, G. Worth, and H.-D. Meyer, *Physics Reports* **324**, 1 (2000).
- [40] G. W. King, R. M. Hainer, and P. C. Cross, *J. Chem. Phys.* **11**, 27 (1943).
- [41] L. B. Ballentine, *Quantum Mechanics: A Modern Development* (World Scientific, Singapore, 1998).
- [42] J. L. Hansen, J. J. Omiste, J. H. Nielsen, D. Pentlehner, J. Küpper, R. González-Férez, and H. Stapelfeldt, *J. Chem. Phys.* **139**, 234313 (2013).